

# Design of a nanomechanical fluid control valve based on functionalized silicon cantilevers: coupling molecular mechanics with classical engineering design

Santiago D Solares, Mario Blanco and William A Goddard III<sup>1</sup>

Materials and Process Simulation Center, California Institute of Technology,  
Mail Code 139-74, Pasadena, CA 91125, USA

E-mail: wag@wag.caltech.edu

Received 25 June 2004

Published 23 August 2004

Online at [stacks.iop.org/Nano/15/1405](http://stacks.iop.org/Nano/15/1405)

doi:10.1088/0957-4484/15/11/004

## Abstract

Process engineering design relies on a host of mechanical devices that enable transport phenomena to take place under controlled conditions. These devices include pipes, valves, pumps, chemical reactors, heat exchangers, packed columns, etc. Mass, energy, and momentum transfer will also be essential phenomena in nanoprocess engineering, particularly at the interface between micro- and nanodevices. Control valves are one of the most fundamental components. In this paper we explore the design of a silicon cantilever valve for fluid transport control at the molecular level (34.5–70 nm in length). We utilize design elements that can be synthesized with existing or emerging chemical and solid state fabrication methods. Thus, the valve is constructed with functionalized silicon surfaces, single-wall carbon nanotubes, and organic monolayers. While molecular mechanics design limitations were overcome with help from classical engineering approximations, nonlinear effects, such as nanotube crimping (for an in-line valve design), are accounted for through full-physics atomistic simulations. Optimal design geometries and operating deflection ranges have been estimated for a device containing over 75 000 atoms.

(Some figures in this article are in colour only in the electronic version)

## 1. Introduction

In the last few years there have been significant advances in the characterization of the mechanical properties of carbon nanotubes, silicon and silicon oxide surfaces and cantilevers [1–4]. Properties such as resonance frequency and bending modulus have been extensively researched for both cantilevers and carbon nanotubes [1, 5–8]. A great deal of work has also been done on the mechanical properties of

functionalized cantilevers, generally covered on one face with a metallic layer of variable thickness and composition, polymer coatings, or monolayers of self-assembled or chemically bonded molecules of various types [8–16]. Functionalized cantilevers exhibit deflection due to differences in surface stress between functionalized and non-functionalized opposite faces. The surface stress on the functionalized face is a function of the environment, and the changes induced by the environment are generally reversible. Since it is possible to control the environment, it is also possible to generate

<sup>1</sup> Author to whom any correspondence should be addressed.

controlled deflection of the cantilever. This presents significant opportunities to utilize functionalized cantilevers as reliable and reversible actuators in nanomechanical devices such as valves, pumps, switches, etc.

In this paper we present the design of a fluid control valve that utilizes a silicon cantilever, functionalized with a covalently bonded monolayer of acrylic acid, as the actuator that opens and closes flow through a fluid conduit, a single-wall carbon nanotube (SWNT). The on/off position of the valve is controlled by pH changes in the surrounding environment. Changes in pH affect the charge of the organic acid groups bonded to the surface of the cantilever. The electrostatic energy of these acid groups on the functionalized surface of the cantilever causes a compressive stress that deflects it to the closed position [10]. The device assembly and valve components are feasible with today's laboratory synthesis capabilities (SWNT synthesis methods, silicon etching techniques and covalent monolayer assembly).

Classical engineering design approximations can be utilized to lower the computational costs of current molecular modelling methodologies. As devices become larger, their design becomes computationally more expensive and in some cases impractical (an  $N^2$  problem). In the present case, for example, the system has in excess of 75 000 atoms and is over 30 nm long. Since the performance of the system depends on the electrostatic interaction of *all* the functional molecules on the surface of the device, it is necessary to include in the calculations *all* the electrostatic interactions of *all* charged particles in order to have an accurate model. Efficient electrostatic lattice sum methods, such as Ewald and Particle-Mesh Ewald, cannot be employed without introducing artefacts due to the imposition of periodic boundary conditions (the device under consideration is not a periodic system); thus we are left with a direct electrostatic sum in real space. In most standard molecular simulation packages this would require including all non-bonded interactions within a radius of 30 nm. Since the number of non-bonded interactions scales as  $N^2$ , this makes the calculations unnecessarily lengthy assuming that the computing system has enough memory to store such a large energy expression. Furthermore, the use of cutoffs or splines in the calculation of the electrostatic energy can underestimate the correct values by factors of one order of magnitude for the monolayer dimensions considered here.

A second computational issue is the statistical nature of the evaluation of the convergence criteria used in a molecular mechanics simulation. Average forces or strain energies do not necessarily represent the equilibrium state of the system, local or global. Due to the large number of atoms, large residual forces and stresses may be present in a small section of the system, while the average force and strain are quite small. A criterion based on average forces/strains may leave the device in a non-equilibrium state.

These difficulties will be overcome with more powerful computer systems and more flexible molecular simulations software packages, but this requires time, human and financial resources, and breakthroughs in computer systems. A more practical approach is to perform a semi-continuum characterization of the system, whereby each component of a particular device is individually characterized using molecular simulations prior to a classical analysis of the entire

device. This characterization includes the determination of the classical engineering parameters needed for the continuum analysis, such as natural vibrational frequencies, elasticity moduli, and points of mechanical failure, at the length scale under consideration. Once these parameters are available, the continuum analysis of the assembled device becomes a simple exercise. The latter approach is presented in this paper.

It must also be noted that in order to have a complete *ab initio* description of the device presented here, there are several fundamental issues that still need to be answered. Two of them are the molecular transport phenomena through SWNTs and the solvation properties of acid monolayers on deflected cantilevers. Although no attempt is made to resolve these issues in this paper, the engineering method presented here remains a useful design tool for the future inclusion of these effects. This is because it is generally possible to find smooth-varying mathematical approximations of those effects, over finite length and timescales, which can then be incorporated into the engineering continuum models. Atomistic simulations provide the range over which these smooth approximations are valid as well as identifying the regions where transitions take place. A prime example of a complex system which can be classically approximated with segment-wise smoothly varying functions is the bending of an SWNT, which exhibits buckling phenomena (see figure 6 below).

## 2. Design concept and potential applications

The present design (see figure 1) consists of a silicon block and cantilever, which is functionalized on its top surface to provide a layer where electrostatic repulsion can take place. We initially chose to functionalize the cantilever with a covalently bonded organic monolayer made of acrylic acid, although other possibilities are discussed below (such as the electrostatic deflection of charged metallic mono- or bilayers on the surface of the cantilever).

The organic monolayer can be assembled on the surface through hydrogenation of the cantilever, followed by thermal reaction of the hydrogenated surface with the olefin of the acid. The silicon block can be etched to its final dimensions, and then its lower part can be perforated so that an SWNT can be inserted through the perforation. The SWNT is used as the fluid transport conduit, which may be connected to other devices as part of a larger system. The choice of a covalently bonded monolayer ensures that the structure of the device will be stable and will not be subject to undesirable changes by the solution environment.

Depending on whether the discharge end of the valve is fixed or movable, two designs are considered here (see figure 2):

- (a) an 'in-line' design, where the discharge end of the SWNT is connected to another device and therefore it is not allowed to move. In this case, it is required that there be a surface on which the SWNT rests, so that the action of the cantilever 'crimps' the SWNT against that surface in order to interrupt the flow through it; and
- (b) a 'free-end' design, where the position of the discharge end of the SWNT is not constrained, and the action of the

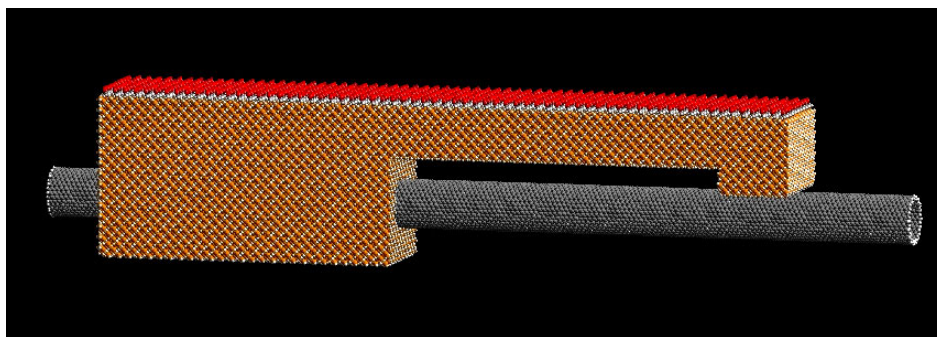


**Figure 1.** Side view of the nanomechanical valve, showing the silicon block construction, the acrylic acid monolayer on the top surface and a 17, 17 SWNT inserted through the silicon block. The model shown contains approximately 76 500 atoms and its main body (silicon block) is 35 nm long.

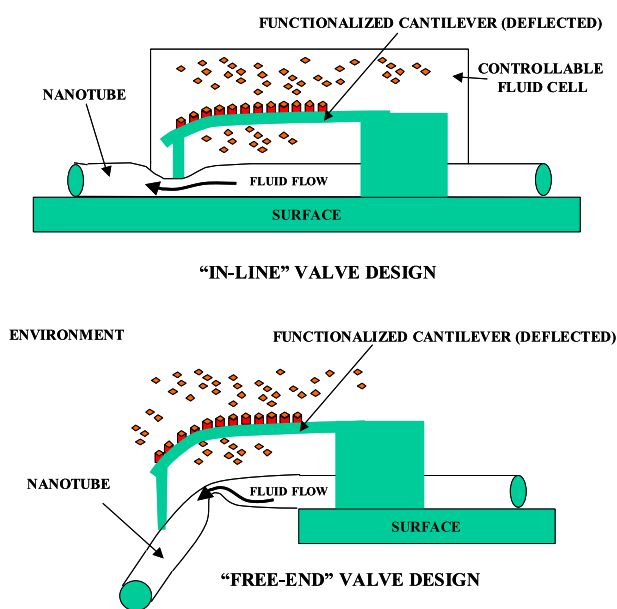


**Figure 2.** Two types of valve design according to the mobility of the discharge end of the nanotube: ‘in-line’ and ‘free-end’ designs.

cantilever deflects the SWNT past the point of buckling, thus interrupting the flow.

The device shown in figure 1 is designed to work in an aqueous environment (although this is not the case for systems relying on the deflection of charged metallic layers). If the pH of the surrounding environment is low, most of the molecules on the monolayer will be protonated and as a result there will not be a significant net charge on the monolayer. There may be a slight stress on the surface due to the van der Waals interactions between monolayer molecules, which may very slightly deflect the cantilever up or down, but this will have only a negligible effect on the flow through the SWNT. If the pH of the surrounding environment is high, a certain amount of molecules on the monolayer will deprotonate, resulting in a net negative charge on the surface of the cantilever. The excess charge will cause a compressive stress that will deflect the cantilever downwards [10], thus exerting pressure on the SWNT and interrupting the fluid flow. Since changes in pH are reversible (by addition of acids and bases) and the device structure is inert to the environment, the process is repeatable.

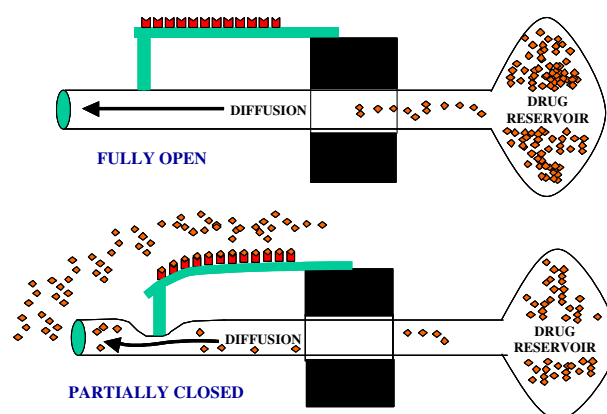


**Figure 3.** Self-regulated dosing of acid and basic compounds (e.g. drugs).

It is also worth noting that the section of the monolayer assembled behind the cantilever, on the non-deflecting part of the valve (main silicon block), is a necessary design element in order to force the cantilever to deflect downwards. If the monolayer stopped behind the base, the cantilever would be relatively free to curl in an inverted ‘U’ shape rendering it inadequate to interrupt the flow through the SWNT. Basically, the section behind the cantilever overcomes most of the upward torque around the base, which comes from the force exerted on its tip by the SWNT.

In the short term, our valve design has multiple potential uses in nanofluidics, including fields such as medicine, biology, environmental engineering, micro- or nanoengines, ink-jet printing, and any other application where fluid transport is desired at the nanoscale level. In addition, this device can be set up for self-regulated dosing of compounds (see figure 3). This can be achieved by connecting the device to a reservoir containing the reactant, so that after flowing out through the SWNT, the reactant changes the pH of the surrounding environment, thus causing the valve to close until the pH has returned to the level that allows it to open again. The process could continue until the reservoir is completely empty.

In the long term we envision the control valve presented here as a key element at the interface between micro- and nanoscale devices. For example, fluid transport between microstorage tanks, for reactants and products, and position controlled nanosynthesis devices, will require control

**Table 1.** Force field energy expression [17, 18]. The force field used for each energy contribution is listed in parentheses.

	$E = E_{\text{bond stretch}} + E_{\text{angle bend}} + E_{\text{torsion}} + E_{\text{inversion}} + E_{\text{van der Waals}} + E_{\text{electrostatic}}$
Total energy	
Bond stretch energy (Universal)	$E_r = \frac{1}{2}K_r(R - R_0)^2$
Angle bend energy (Universal)	$E_\theta = \frac{1}{2}\frac{K_\theta}{\sin^2\theta_0}(\cos\theta - \cos\theta_0)^2$
Torsion energy (Dreiding)	$E_\phi = \frac{1}{2}V(1 - d \cos n\phi)$
Inversion energy (Dreiding)	$E_\psi = K_\psi(1 - \cos\psi)$
van der Waals energy (Universal)	$E_{\text{vdw}} = D_0\left(\left(\frac{R}{R_0}\right)^{-12} - \left(\frac{R}{R_0}\right)^{-6}\right)$
Electrostatic energy (classical) <sup>a</sup>	$E_Q = 322.0637 \sum_{i>j} \frac{Q_i Q_j}{\epsilon R_{ij}}$

<sup>a</sup> Energies in kcal mol<sup>-1</sup>, charges in electronic units and distances in ångströms.

mechanisms such as the valve designed here to regulate the throughputs of fluid species.

### 3. Design methodology

#### 3.1. Design overview

Classical engineering design makes use of bulk material properties, such as Young's modulus, heat capacity, heat conductivity, diffusion coefficients, etc. These properties have more fundamental energy and force components at the atomistic level, such as electrostatic and van der Waals interactions, as well as covalent intramolecular interactions. These properties are embedded in classical force fields, mathematical expressions for the energy and forces within a molecular system given the charges and positions of all atoms. In turn, the parameters in the force field depend on the nuclear and electronic structure of the molecules, which can be estimated using quantum mechanics [17, 18].

In order to have an accurate description of a nanodevice it is desirable to include as much molecular detail as possible in the analysis of its behaviour. However, for the reasons described above it is not practical to conduct all design steps at the molecular level. Hence, we present a hybrid methodology that combines molecular simulations with classical engineering. The molecular simulations provide the elastic and/or electrostatic properties of each component of the system considered individually, estimated from the force field, while the classical analysis provides the behaviour of the assembled system based on those properties. In summary the steps followed in the present design are the following.

#### Molecular simulation steps:

- (1) Selection of force field parameters for the elements included in the design.
- (2) Selection of a monolayer.
- (3) Evaluation of the Young's modulus of silicon at the length scale of the actuator cantilever.
- (4) Selection of the SWNT and evaluation of its strain energy function and point of mechanical failure (buckling) in the appropriate range of curvature (for 'free-end' designs).
- (5) Evaluation of the SWNT crimping energy as a function of the inner opening (for 'in-line' designs).

**Table 2.** Force field atom types.

H_	Hydrogen
H__A	Acid hydrogen
C_3	Tetrahedral carbon (sp <sup>3</sup> )
C_R	Resonant carbon
C_2	Planar carbon (non-resonant sp <sup>2</sup> )
O_3	Tetrahedral oxygen
O_R	Resonant oxygen
O_2	Planar oxygen (non-resonant sp <sup>2</sup> )
Si3	Tetrahedral silicon

**Table 3.** Force field bond stretch parameters. See table 1 for the energy expression. Parameters from the Universal force field [17].

Atom 1	Atom 2	$K_r$	$R_0$
C_3	H_	662.9963	0.7080
C_3	C_3	699.5920	1.5140
C_R	H_	715.3873	1.0814
C_R	C_3	739.8881	1.4860
C_R	C_R	925.3104	1.3793
C_2	H_	709.4702	1.0844
C_2	C_3	735.4249	1.4890
O_3	H_	1120.7078	0.9903
O_3	C_3	1078.4241	1.3938
O_R	H_	1049.6934	1.0121
O_R	C_2	1085.0881	1.391
O_2	C_2	1610.4076	1.2195
O_2	C_R	1153.3079	1.3630
O_3	H__A	500.0000	1.0000
Si3	H_	345.6964	1.4930
Si3	C_3	453.3563	1.8669
Si3	Si3	321.4845	2.3650

- (6) Evaluation of the electrostatic energy of the monolayer as a function of cantilever curvature and dimensions for various levels of charge density (pH).

#### Classical engineering steps:

- (1) Valve assembly and geometry optimization.
- (2) Evaluation of the mechanical properties of the charged cantilever as a function of curvature and dimensions.
- (3) Evaluation of the mechanical properties (strain energy and forces) acting within the assembled device as a function of monolayer charge, device geometry and curvature of the components, and determination of ranges of operation as well as equilibrium geometries.

#### 3.2. Design details

##### Molecular simulation steps:

- (1) *Selection of force field parameters.* Extensive documentation is available on the accuracy and applicability of existing force fields. The present analysis was conducted using the Universal force field [17] with two modifications:
  - (a) the silicon-silicon bond length parameter was corrected in order to match the lattice parameters of the silicon crystal, and
  - (b) the torsion and inversion terms were taken from the Dreiding generic force field [18].

**Table 4.** Force field angle bend parameters. See table 1 for the energy expression. Parameters from the Universal force field [17].

Atom 1	Atom 2	Atom 3	$K_\theta$	$\theta_0$
H_	C_3	H_	75.2779	109.4710
C_3	C_3	H_	117.2321	109.4710
C_3	C_3	C_3	214.2065	109.4710
C_2	C_3	H_	121.1966	109.4710
C_2	C_3	C_3	219.5725	109.4710
O_3	C_3	H_	160.9632	109.4710
O_3	C_3	C_3	284.0680	109.4710
Si3	C_3	H_	89.6088	109.4710
Si3	C_3	C_3	181.9182	109.4710
C_R	C_R	H_	103.1658	120.0000
C_R	C_R	C_R	188.4421	120.0000
C_R	C_3	H_	121.6821	109.4710
C_R	C_3	C_3	220.2246	109.4710
C_3	C_2	H_	98.7841	120.0000
C_3	C_R	O_2	242.4495	120.0000
O_R	C_2	C_3	229.9906	120.0000
O_2	C_2	H_	139.6784	120.0000
O_2	C_2	C_3	240.9266	120.0000
O_2	C_2	O_R	315.2170	120.0000
O_2	C_R	O_2	333.7212	120.0000
C_3	O_3	H_	165.6001	104.5100
H_	O_3	H_	113.0577	104.5100
C_2	O_R	H_	142.0707	110.3000
H_	Si3	H_	32.4318	109.4710
C_3	Si3	H_	57.6239	109.4710
Si3	Si3	H_	48.9079	109.4710
Si3	Si3	C_3	102.7429	109.4710
Si3	Si3	Si3	98.4346	109.4710
H_A	O_3	H_A	120.0000	109.4710

**Table 5.** Force field torsion parameters. See table 1 for the energy expression. Parameters from Dreiding force field [18].

Atom 1	Atom 2 (centre 1)	Atom 3 (centre 2)	Atom 4	$V$	$n$	$d$
Any	C_3	C_3	Any	2.0000	3	-1
Any	C_R	C_R	Any	25.0000	2	1
Any	C_2	C_3	Any	2.0000	3	-1
Any	O_3	C_3	Any	2.0000	3	-1
Any	O_R	C_2	Any	25.0000	2	1
Any	Si3	C_3	Any	2.0000	3	-1
Any	Si3	Si3	Any	2.0000	3	-1
Any	C_R	C_3	Any	2.0000	3	-1

**Table 6.** Force field inversion parameters. See table 1 for the energy expression. Parameters from Dreiding force field [18].

Atom 1 (centre)	Atom 2	Atom 3	Atom 4	$K\psi$	$\psi_0$
C_R	Any	Any	Any	6.0000	0.0000
C_2	O_2	Any	Any	50.0000	0.0000

Tables 1–7 summarize the atom types, force field energy expression, and force field parameters used in the characterization of the device described here.

- (2) *Selection of the monolayer.* Various chain lengths of the carboxylic acids (C<sub>3</sub>, C<sub>6</sub>, C<sub>12</sub> and C<sub>20</sub>) and surface geometrical arrangements (linear, zig-zag and hexagonal) were considered on the Si(111) surface at 50% coverage. This was necessary in order to assess the magnitude of the forces on the cantilever beam due to the interactions between the closely packed molecules of the monolayer.

**Table 7.** Force field diagonal van der Waals parameters (see table 1 for the energy expression). Parameters describing the interaction of dissimilar atoms were estimated using the geometric combination rule:  $A_{ij} = (A_i \times A_j)^{0.5}$ . A third degree polynomial spline function was used with cut-on = 11.0 Å and cut-off = 14.0 Å for van der Waals interactions between atoms separated by 11.0 Å or more. Parameters from the Universal force field [17].

Atom	$R_0$	$D_0$
H_	2.8859	0.043999
H_A	0.8999	0.009999
C_3	3.8510	0.104999
C_R	3.8510	0.104999
C_2	3.8510	0.104999
O_3	3.5000	0.059999
O_R	3.5000	0.059999
O_2	3.5000	0.059999
Si3	4.2950	0.402000

The calculations were repeated for the same percentage of coverage using the Si(100) surface and the C<sub>3</sub> monolayer (note that the density of molecules on the Si(100) surface is lower than on the Si(111) surface at 50% coverage). In each case the monolayer cohesive energies were calculated through molecular simulations. Due to the more negative cohesive energy of longer carbon chains (which would oppose the deflection of the cantilever) and due to its having its carboxylic acid groups closest to the surface, an acrylic acid monolayer (C<sub>3</sub>) was selected. Very little strain is stored in the short hydrocarbon tail of this acid. The choice of a monolayer that brings the carboxylic groups close to the surface also facilitates the modelling of the system by restricting the motion of these groups. Finally, the Si(100) surface was selected versus the Si(111) due to the complex reconstruction that the latter undergoes, which makes it difficult to work with, and the orthogonal symmetry of the Si(100) surface, which prevents the cantilever from twisting during deflection. The results of the cohesive energy study for the Si(111) surface are shown in figure 4. It is not necessary to evaluate different geometries of the Si(100) surface because there is only one possible uniform arrangement at 50% coverage.

- (3) *Evaluation of the Young's modulus of silicon at the length scale of the actuator cantilever.* A series of molecular mechanics simulations of 15 nm × 3 nm × 2 nm cantilevers ( $L \times W \times H$ ) at various levels of curvature ( $R_c^{-1}$ , where  $R_c$  is the radius of curvature) were conducted using the Si(100) and Si(111) hydrogen terminated surfaces, and their strain energy curves were constructed as a function of the curvature. Utilizing classical elasticity approximations and simple regression techniques, the Young's modulus of the material was calculated. Knowledge of the Young's modulus allows the construction of cantilevers of various sizes and the classical analysis of their strain energies and deflection forces as a function of curvature (see figure 5).
- (4) *Selection of the SWNT and evaluation of its strain energy function and point of mechanical failure (buckling) in the appropriate range of curvature (for 'free-end' designs).* The selection of the SWNT size should be based on the desired fluid flow rates and the size of the molecule that is flowing through it. Based on molecular simulations, it is

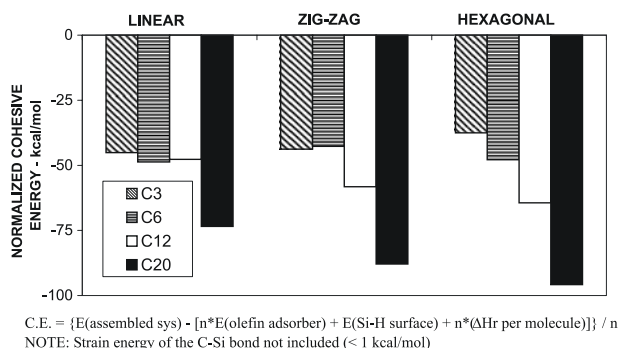


**Figure 4.** Analysis of monolayer cohesive energy (normalized to the number of adsorbed molecules) for three different geometrical arrangements of four organic acids (acrylic, hexanoic, dodecanoic and eicosanoic) on an Si(111) surface at 50% coverage. The results show increasing monolayer stability (more negative cohesive energy values) with increasing carbon chain length. As shown on the graph, the linear arrangement was more stable at shorter chain lengths, while the hexagonal arrangement was more stable for longer chain lengths. Note that the monolayer cohesive energy opposes the cantilever deflection.

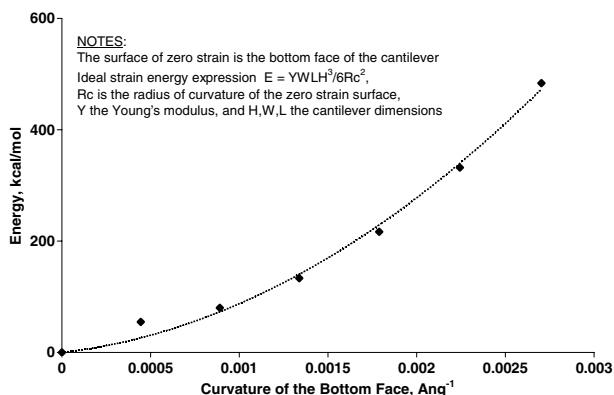


**Figure 5.** Strain energy as a function of curvature ( $R_c^{-1}$ ) for the  $15 \text{ nm} \times 3 \text{ nm} \times 2 \text{ nm}$  cantilever. Note that the plane of zero deformation is at the bottom face of the cantilever (as occurs when compressive stress is present on the top face). The average Young's modulus for silicon calculated from the above strain energy curve is 76.7 GPa versus the experimental bulk value of 47 GPa.

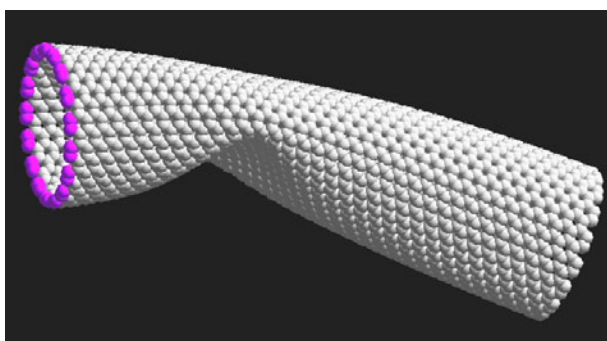


**Figure 6.** 17, 17 carbon nanotube under elastic bending at a curvature of  $0.0031 \text{ \AA}^{-1}$  (beyond the point of buckling). This nanotube will return to its original (straight) conformation upon removal of the stress applied to bend it.

known that SWNTs are most stable with a circular cross section up to a radius of approximately 3 nm [1]. Larger

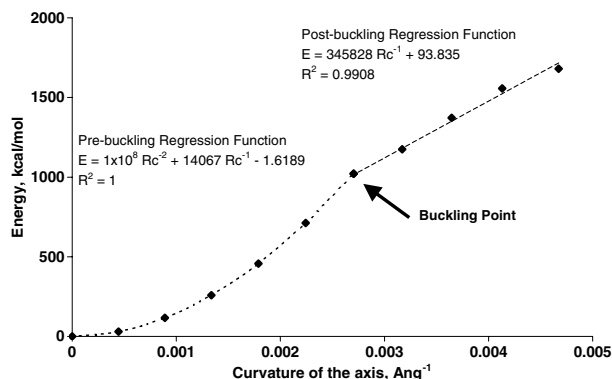


**Figure 7.** Strain energy as a function of curvature ( $R_c^{-1}$ ) for the nanotube shown in figure 6. The graph shows two distinct strain energy functions below and above the point of buckling.

radii yield tubes that are more stable in the collapsed conformation. Estimates of the strain energy for the SWNT as a function of curvature are necessary if the discharge end of the valve is allowed to move, as in the 'free-end' design shown in figure 2. It is also necessary to determine the value of the curvature at which the SWNT buckles and completely interrupts the flow through it. For this particular design a 17, 17 SWNT was selected, the radius of which is within the region where SWNTs are most stable with round cross sections (radius = 1.15 nm). A 17, 17 SWNT could be used to transport a variety of fluids such as nitrogen, water, benzene, cyclohexane and n-octane, all of which have molecular dimensions smaller than 1.15 nm. The molecular simulations showed that when bent, the 17, 17 SWNT deflects uniformly up to a curvature of approximately  $0.0027 \text{ \AA}^{-1}$ , after which it buckles. Figure 6 shows a 17, 17 SWNT at the point of buckling and figure 7 shows the strain energy results as a function of curvature, including the point of buckling.

- (5) *Evaluation of the SWNT crimping energy as a function of the inner opening (for 'in-line' designs).* The energy of the SWNT was determined for different levels of 'crimping', from completely open to completely closed. The size of the 'crimped' section is comparable to the contact area the tube would have when the cantilever is fully deflected. The energy curves as a function of the internal opening and cantilever curvature for the 17, 17 SWNT are summarized in figures 9 and 10. Figure 8 shows a partial view of the model used to determine the crimping curve of the device. It consists of a section of 17, 17 SWNT plus the tip of an Si(100) cantilever. Note that the strain energy curve also includes the deformation experienced by the tip of the cantilever.
- (6) *Evaluation of the electrostatic energy of the monolayer as a function of cantilever curvature.* The last and largest energy contribution to the operation of the device is the electrostatic energy. The electrostatic energy was computed as the energy of a grid of point charges, where the location of each point charge corresponded to the lattice position of each adsorbate molecule on the Si(100) surface. The vertical position of the charges above the cantilever surface was set to a value equal to the height of the oxygen atoms of the deprotonated carboxylic

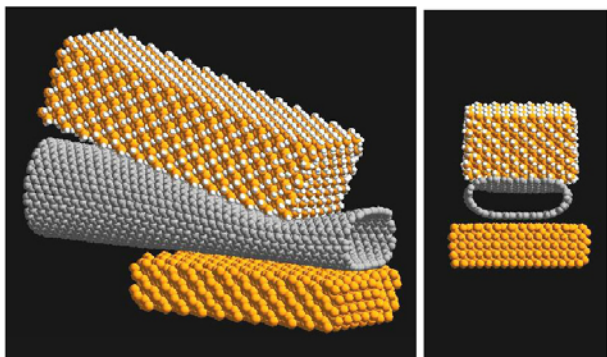


**Figure 8.** Partial view of the model used to construct the crimping energy curve, showing the tip of the cantilever, part of the 17, 17 nanotube and part of the Si(100) surface on which the system rests.

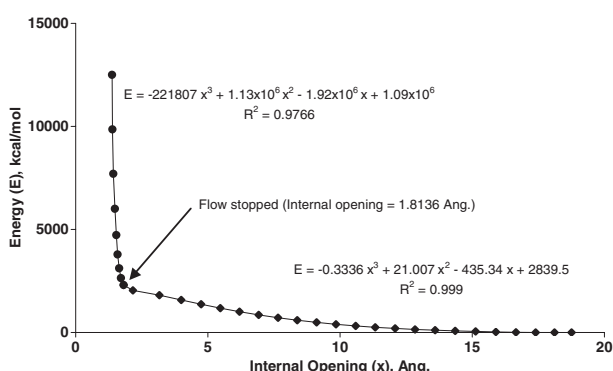


**Figure 9.** Strain energy as a function of the internal opening of the carbon nanotube for the model shown in figure 8. Note the sharp change in the slope of the curve at approximately 1.81 Å of internal opening. The amount of energy required to crimp the nanotube below this value increases exponentially according to the force field short-range van der Waals functions [17]. For the classical analysis of the present device it was assumed that no fluid flows through the nanotube below this value. As shown in figure 11, this is a reasonable assumption based on the energy required for a molecule to flow from one side of the crimped section to the other.

acid molecule above the cantilever. The positions of the point charges for deflected cantilevers were found through simple geometrical calculations, taking into account the cantilever curvature, and the height of the charges above the plane of zero deformation of the curved cantilever. Each point charge was assigned one electron charge, which corresponds to complete deprotonation of the carboxylic acid groups (at this stage we have not considered solvent effects, although we have analysed partial deprotonation states). The energy calculation was repeated for various levels of cantilever curvature in order to obtain a function that relates the electrostatic energy of the cantilever (with the assumptions listed above) to its curvature. At this point two fundamental questions arise: What is the net charge on each molecule of the monolayer and what is the effect of the surrounding environment on the electrostatic interactions between all molecular pairs? Although this topic is not treated in this paper, the present analysis allows for the introduction of correction factors to the total electrostatic energy if additional knowledge regarding the total charge of the system or the effect of the solvent is available. Charge scaling effects are

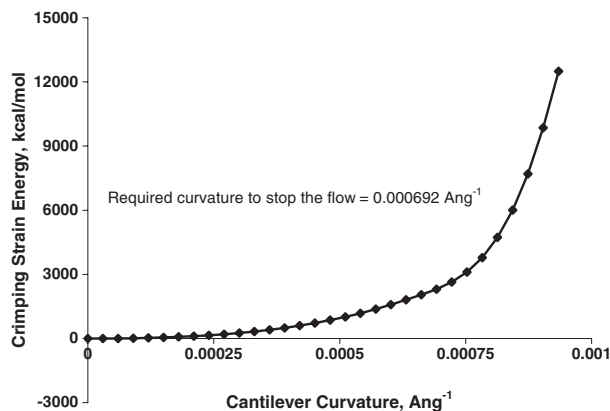


**Figure 10.** Strain energy (due to crimping of the nanotube) versus curvature of the cantilever for the model shown in figure 8. The y-axis values used to construct this graph correspond to the energy values of the graph in figure 9 (crimping energy as a function of internal opening). The x-axis value for each point corresponds to the curvature that the cantilever would have in order to crimp the nanotube up to that point. The curvature of the cantilever was determined through geometrical calculations based on its displacement towards the nanotube and assuming that it has a uniform curvature throughout its length.

proportional to  $q^2$ , where  $q$  is the net charge on each carboxylic acid group, and the correction for solvent effects can be introduced in the form of a dielectric constant. This assumes that all carboxylic acid groups on the monolayer have the same charge, hence all energy terms considered in the calculation of the electrostatic energy are of the form  $Kq^2/r$ , where  $K$  is a constant that includes the dielectric constant of the surrounding environment and  $r$  is the distance between pairs of charged molecules. Figure 12 shows the electrostatic energy as a function of curvature for a 22.5 nm × 6 nm × 2 nm ( $L \times W \times H$ ) cantilever completely deprotonated and without solvent effects.

#### Classical engineering steps:

- (1) *Valve assembly, geometry and different attachment systems.* Different ways of assembling the valve were evaluated for chemical feasibility and ease of assembly. Several of them included the attachment of the silicon cantilever to the SWNT through SWNT–silicon junctions; however, the chemical feasibility of these designs is quite low, and there are no manufacturing procedures that guarantee that such devices could be produced efficiently and with high yields with current chemical synthesis methods. The chosen design consists of a perforated block of silicon through which the SWNT is inserted. The insertion of the SWNT through the block of silicon can be a difficult operation in itself, depending on the size of the opening, but there is no need to make that opening as small as the SWNT, as long as the relative position of the tube with respect to the cantilever is accurately fixed. Alternatively, the SWNT could be generated *in situ* through placement of catalytic metal particles inside the silicon cavity prior to etching the silicon block to its final dimensions.

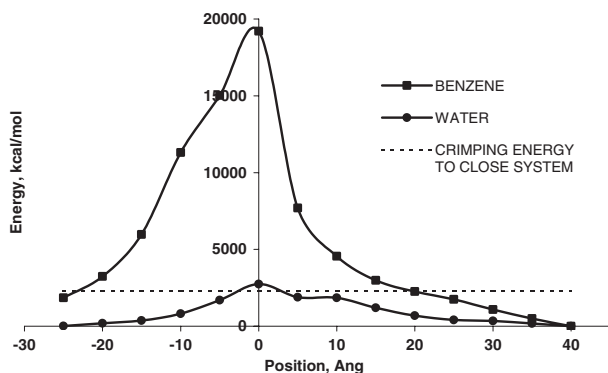


**Figure 11.** Incremental energy of the 'in-line' valve system due to the presence of a *single* molecule moving through the crimped section (throat) of the 17, 17 nanotube when the minimum opening (skin to skin) is 1.81 Å. The results show that the incremental energy of the system due to the presence of a single molecule at the valve throat is above the total crimping energy for the system (see figures 9 and 10), hence it is reasonable to consider this as the closed position of the valve. Note: the zero energy of the graph corresponds to the lowest energy of each molecule during the trajectory analysed.

(2) *Evaluation of the mechanical properties of a charged cantilever as a function of cantilever curvature and dimensions.* The quantities of interest regarding the performance of the device are the energy and forces that the cantilever is capable of exerting at different levels of curvature within its operational range of deflection. A high-performance cantilever will be one whose potential energy is high in the undeflected state, with a steep gradient towards high curvatures (in the charged state). Thus, the cantilever is capable of exerting a large force in the direction of deflection. The total energy of the cantilever was calculated as the sum of its strain energy and the electrostatic energy of the charges distributed on it, both of which had been previously calculated as a function of curvature using molecular simulations. Clearly, as the curvature of the cantilever increases, the strain energy of the material increases, while the electrostatic energy decreases until the point of equilibrium where these balance each other. The force is the derivative of the total energy of the cantilever as a function of the displacement along the path of motion. A 15 nm × 3 nm × 2 nm Si(100) cantilever, for example, would be capable of a maximum downward force of approximately 7.5 nN if the monolayer of acrylic acid on its top surface (50% coverage) were completely deprotonated in vacuum. This force would decrease to approximately half of that value if the tip were allowed to deflect 5 nm vertically (a third of the length of the cantilever). The forces the same cantilever would be able to exert in a solution environment would of course be lower than that according to the dissociation properties of the monolayer and the pH of the solution. It is important to note that the strain energies of the cantilevers must be calculated by stretching the top (charged) surface of the cantilever while the bottom surface remains at its original length, which is the effect that a compressive stress on the top surface would cause. This mode of deflection is different from the deflection of a cantilever through the application of a force to its

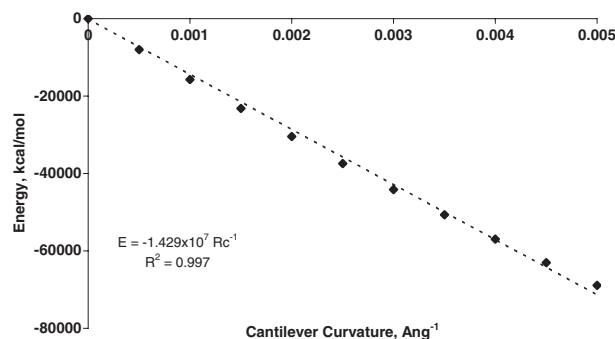


**Figure 12.** Electrostatic energy as a function of cantilever curvature ( $R_c^{-1}$ ) for a 22.5 nm × 6 nm × 2 nm ( $L \times W \times H$ ) cantilever completely deprotonated without including solvent effects. The electrostatic energy calculations in this analysis include all the net charges on the surface. No cutoffs or spline functions were used, for the reasons discussed in the text.

tip. In the latter mode, the top surface stretches and the bottom surface compresses by similar amounts, while the plane of zero deformation runs through the middle of the cantilever (between the top and the bottom surfaces). The former mode of deflection corresponds to strain energies four times greater than the latter mode according to ideal elasticity calculations.

(3) *Evaluation of the mechanical properties of the assembled valve as a function of monolayer charge and curvature of the components.* As in the previous case, the total energy of the system can be found by adding the partial energy contributions of the components. The total energy of the system is the sum of the total energy of the cantilever (charge and strain as previously calculated) plus the deformation (strain) energy of the SWNT, whether due to deflection or crimping. The strain energy of the SWNT needs to be supplied by the charged cantilever. In order to have a working system it is only required that the electrostatic energy available for deflection exceeds the strain energy of the deflected components at the closed position of the valve. Figure 13 shows the partial energy contributions and the total energy of a system that uses a 15 nm × 3 nm × 2 nm cantilever ( $L \times W \times H$ ), which deflects a 'free-end' 17, 17 SWNT. It was assumed that the available electrostatic energy is only 10% of the maximum corresponding to total deprotonation of the system in vacuum (this is equivalent to assuming that there is a net charge of  $-0.32e$  on each carboxylic acid group). The total energy of the system shows a minimum at a curvature of  $0.00085 \text{ \AA}^{-1}$ , which is not enough to deflect the SWNT to the point of buckling (curvature of  $0.0027 \text{ \AA}^{-1}$ ). Thus this system is not capable of interrupting the flow through the SWNT. Using the methodology described above, the system was redesigned to include a 22.5 nm × 6 nm × 2 nm cantilever (twice as wide and 50% longer as the original cantilever). The redesign includes recalculating the electrostatic and strain energies of the new (larger) cantilever. The performance of the new system is shown in figure 14 (again, considering that only 10% of the maximum electrostatic energy is available). In this case, the total energy of the system does not exhibit a minimum in the range of curvature evaluated,

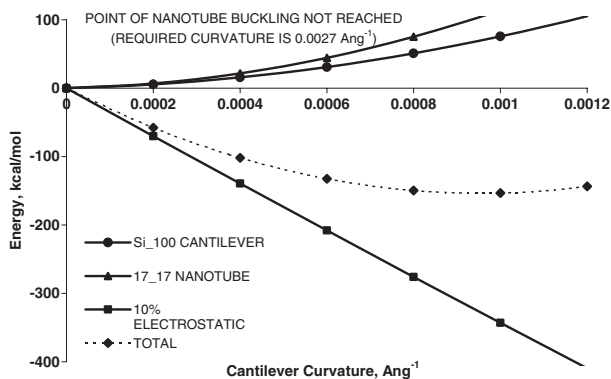


**Figure 13.** Performance chart of a cantilever valve, showing the partial energy contributions and the total energy of a system with a  $15 \text{ nm} \times 3 \text{ nm} \times 2 \text{ nm}$  cantilever ( $L \times W \times H$ ). This corresponds to a ‘free-end’ design with a 17, 17 SWNT. It is assumed that the available electrostatic energy is only 10% of the maximum (i.e. each carboxylic acid group has a charge of approximately  $-0.32e$ ). As shown, the system is *not* able to reach the point of buckling of the SWNT, which occurs at a curvature of  $0.0027 \text{ \AA}^{-1}$ .

and the cantilever *is* capable of deflecting the SWNT past the point of buckling. Figure 15 shows the same analysis for an ‘in-line’ design. This requires the use of the SWNT ‘crimping’ energy curve instead of the deflection energy curve. In this case, however, the working design required a  $45 \text{ nm} \times 9 \text{ nm} \times 2 \text{ nm}$  cantilever (three times as long and three times as wide as the original cantilever), which has three times the monolayer surface area as the cantilever used in the ‘free-end’ design. Note that the length of the silicon block holding the cantilever needs to be added to the length of the cantilever to obtain the total length of the system. If the length of this block is set at 10 nm, for example, then a feasible ‘free-end’ design would be 32.5 nm long and a feasible ‘in-line’ design would be 55 nm long.

#### 4. Discussion

The coupling of molecular simulations and engineering principles as described here has the following advantages.

- (1) *Atomic detail accuracy on individual component performance.* Since the properties of the components have been determined through molecular simulations, the energy contributions of the different components are as accurate as the force field parameters used for their estimations. Due to the large number of atoms in each component, and given that the molecular simulation is classical, there should be no significant loss of accuracy in the calculations when the different energy contributions of the system components are calculated separately and then added. In practice, these potential losses in accuracy are taken into account through the appropriate engineering safety factors. In order to have a robust working system it is not necessary to know the exact position of every atom, as long as it is known with certainty that the system will be able to reach the required states under definite controlled conditions: in this case, the valve position (on/off) for specific pH levels of the surrounding environment.

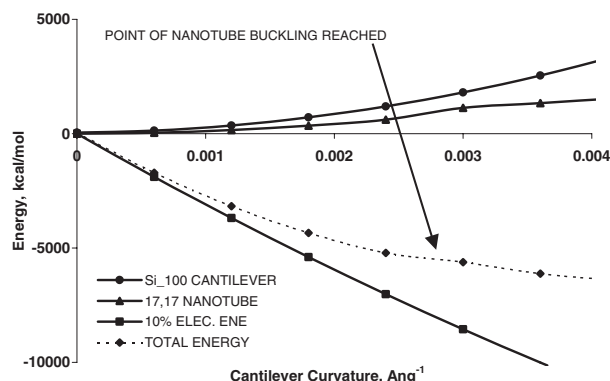


**Figure 14.** Performance chart of a cantilever valve, showing the partial energy contributions and the total energy of a system for a  $22.5 \text{ nm} \times 6 \text{ nm} \times 2 \text{ nm}$  cantilever ( $L \times W \times H$ ). This corresponds to a ‘free-end’ design with a 17, 17 SWNT. It is assumed that the available electrostatic energy is only 10% of the maximum (i.e. each carboxylic acid group has a charge of approximately  $-0.32e$ ). As shown, the system *is* capable of deflecting the SWNT beyond its point of buckling, which occurs at a curvature of  $0.0027 \text{ \AA}^{-1}$ .

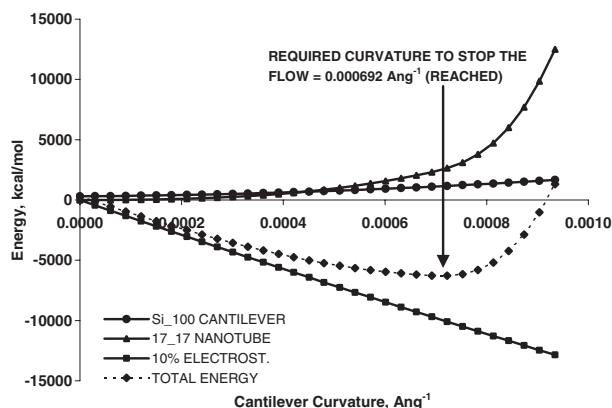


**Figure 15.** Performance chart of a cantilever valve, showing the partial energy contributions and the total energy of a system for a  $45 \text{ nm} \times 9 \text{ nm} \times 2 \text{ nm}$  cantilever ( $L \times W \times H$ ). This corresponds to an ‘in-line’ design with a 17, 17 SWNT. It is assumed that the available electrostatic energy is only 10% of the maximum (i.e. each carboxylic acid group has a charge of approximately  $-0.32e$ ). As shown, the system *is* capable of crimping the SWNT to the point that interrupts the flow through it (the required cantilever curvature to close the valve is  $0.000692 \text{ \AA}^{-1}$ ). Note that the curvature of the cantilever of an ‘in-line’ valve will always be limited by the surface against which the SWNT is crimped. As shown in figure 9, there is a disproportionate increase in the strain energy of the system if it the internal opening of the SWNT is reduced beyond the ‘closed’ position, in this case  $1.81 \text{ \AA}$ . This is because the motion of the cantilever beyond this point starts causing significant deformation of the surface below the SWNT.

- (2) *Scale-up flexibility.* Since the energy curves of the components of the system are smooth varying functions of the relevant parameters (curvature and dimensions), they can be easily incorporated into multiple correlation functions, which allow the design of devices of various length scales (within the ranges for which the data were obtained) without having to repeat the calculations for each individual device.
- (3) *Lower computational cost, especially during prototype development.* The approach presented here requires molec-

ular simulations only during the initial characterization of the components of the system. Once that information is available, modelling of the system becomes a very simple classical physics exercise, which can be completed with negligible computational cost. As research progresses in fundamental areas which govern the behaviour of the valve, such as controlled charge distributions in charged monolayers or response times to changes in pH (monolayer pH curves), these can be easily incorporated into the classical engineering model without significantly increasing the computational cost of prototype development. This provides the design teams with a very accurate and powerful, yet efficient tool for fast prototyping in the laboratory.

## 5. Areas of future research

As mentioned above, there are several fundamental questions which need to be answered in order to obtain accurate *ab initio* predictions of the behaviour of molecular devices that utilize functionalized cantilevers to generate motion. We also point out that there are other ways of generating motion in this device for which the current analysis is still valid.

Areas that need immediate attention to fully characterize these devices include:

- (1) *Monolayer solvation properties.* This includes the prediction of charge distributions for the acid monolayers as a function of the cantilever geometry (curvature and dimensions), and environmental factors (pH, and concentrations and types of species present in the solution in which the monolayer is immersed). The solvation properties of a monolayer are expected to be different than those of the individual acid molecules in solution because
  - (a) the motion of the adsorbed molecules is restricted,
  - (b) the molecules are packed relatively close together, which does not allow the solvent to freely penetrate between the molecules, and
  - (c) the change in energy, with respect to surface charge, depends on the geometry and magnitude of the organic monolayer surface [10].
- (2) *Dynamic testing.* This includes the study of the response times of the system to changes in the parameters that generate motion. It can be anticipated that several local and global factors will influence the dynamic performance of the device. Some of the local factors include the speed of change of the local environment of each molecule (concentration distribution of the different species present), the speed with which charges disperse through the monolayer molecules, and the speed with which the cantilever material yields to deformation. Some of the global factors are the transport phenomena (either natural or forced) that govern the speed with which the externally induced changes made to the environment reach the device, and the speed with which the local distribution of the key parameters, such as ion concentrations, change as a function of the global changes made to the system.
- (3) *Molecular transport phenomena.* This includes the study of momentum transfer and diffusion in constrained regions such as the inside of an SWNT [19]. This will also require

reconciling the behaviour of classical continuum systems with molecular systems, perhaps through the development of new models and parameters to characterize molecular behaviours, which are analogous to the traditional models and parameters used in continuum approximations, such as Newton's law of viscosity or Fick's laws of diffusion. Due to the molecular dimensions of these systems, the studies need to take into account the molecular geometry as well as the detailed intermolecular interactions of both the fluid and the fluid conduit.

- (4) *Other means of generating motion.* Due to the anticipated lag time between the pH changes made to the environment surrounding the device and the actual deflection of the cantilever, the current design is not necessarily of the most responsive type. This characteristic makes it reliable only for on/off systems but not necessarily for continuous flow control systems. There have been significant developments in nanoelectronics (mainly nanowires and switches), which can provide improved ways of generating motion that would allow faster response times and a greater degree of positional control of the device. Electronic operation of the system could be accomplished by replacing the acid monolayer on the cantilever with a metallic layer, which can be charged and discharged through an electronic circuit. Two additional advantages of nanoelectronic systems are that

- (a) they do not require changes in the pH of the solution environment, and
- (b) they are better able to communicate with and be acted upon by external systems through electrical signals.

Electrical signals in turn, offer a much more efficient and ubiquitous way of communication, which can combine input and output signals in the same communication channel.

## 6. Conclusions

We have presented the theoretical design and static characterization of a nanomechanical fluid control valve, 32.5–70 nm in length, that utilizes a functionalized silicon cantilever to generate motion in response to pH changes in the surrounding environment. We have also illustrated the steps and advantages of an engineering design procedure that combines molecular mechanics with classical engineering in the design of nanomechanical systems, thus overcoming the major limitations of both. Finally, we have identified the key fundamental areas of future theoretical research for the characterization of this type of nanosystems, for which the next phase should consist of experimental engineering and assembly.

## References

- [1] Gao G, Cagin T and Goddard W A III 1998 *Nanotechnology* **9** 184–91
- [2] Shen T S, Chan C Y and Chou Y C 1999 *Surf. Rev. Lett.* **6** 97–101
- [3] Bengu E, Plass R and Marks L D 1996 *Phys. Rev. Lett.* **77** 4226–8
- [4] Chen G Y, Thundat T, Wachter E A and Warmack R J 1995 *J. Appl. Phys.* **77** 3618–22

- [5] Krishnan A, Dujardin E, Ebbesen T W, Yanilos P N and Treacey M M J 1998 *Phys. Rev. B* **58** 14013–9
- [6] Miyatani T and Fujihira M J 1997 *Appl. Phys.* **11** 7099–115
- [7] Raitieri R and Butt H J 1995 *J. Phys. Chem.* **100** 15728–32
- [8] Berger R, Delamarche E, Lang H P, Gerber Ch, Gimzewski J K, Meyer E and Güntherodt H-J 1997 *Science* **276** 2021–4
- [9] Berger R, Delamarche E, Lang H P, Gerber Ch, Gimzewski J K, Meyer E and Güntherodt H-J 1998 *Appl. Phys. A* **66** S55–9
- [10] Fritz J, Baller M K, Lang H P, Strunz T, Meyer E, Güntherodt H-J, Delamarche E, Gerber Ch and Gimzewski J K 2000 *Langmuir* **16** 9694–6
- [11] Raitieri R, Nelles G, Butt H-J, Knoll W and Skladal P 1999 *Sensors Actuators B* **61** 213–7
- [12] Fritz J, Baller M K, Lang H P, Rothuizen H, Vettiger P, Meyer E, Güntherodt H-J, Gerber Ch and Gimzewski J K 2000 *Science* **288** 316–8
- [13] Hansen K, Ji H-F, Wu G, Datar R, Cote R, Majumdar A and Thundat T 2001 *Anal. Chem.* **73** 1567–71
- [14] Wu G, Ji H, Hansen K, Thundat T, Datar R, Cote R, Hagan M, Chakraborty A and Majumdar A 2001 *Pcoc. Natl Acad. Sci.* **98** 1560–4
- [15] Baller M K *et al* 2000 *Ultramicroscopy* **82** 1–9
- [16] Lee T R, Carey R, Biebuyck H A and Whitesides G 1994 *Langmuir* **10** 741–9
- [17] Rappé A K, Casewit C J, Colwell K S, Goddard W A III and Skiff W M 1992 *J. Am. Chem. Soc.* **114** 10024–35
- [18] Mayo S, Olafson B and Goddard W A III 1990 *J. Phys. Chem.* **94** 8897–908
- [19] Hummer G, Rasaiah J C and Noworyta J P 2001 *Nature* **414** 188–91